Research

Author for correspondence:
Samantha J. Gibbs
e-mail: s.gibbs@noc.soton.ac.uk

[†]Present address: Environmental Science Program, Mount Allison University, Sackville, New Brunswick E4 L 1A5, Canada.
[‡]Present address: The Lyell Centre for Earth and Marine Science and Technology, Heriot-Watt University, Edinburgh EH14 4AP, UK.

THE ROYAL SOCIETY
PUBLISHING

Warm plankton soup and red herrings: calcareous nannoplankton cellular communities and the Palaeocene–Eocene Thermal Maximum

Samantha J. Gibbs[1], Rosie M. Sheward[1,†], Paul R. Bown[2], Alex J. Poulton[3,‡] and Sarah A. Alvarez[4]

[1]Ocean and Earth Sciences, National Oceanography Centre, Southampton, University of Southampton, Southampton SO14 3ZH, UK
[2]Department of Earth Sciences, University College London, Gower Street, London WC1E 6BT, UK
[3]National Oceanography Centre, Southampton SO14 3ZH, UK
[4]School of Geographical Sciences, University of Bristol, University Road, Bristol BS8 1SS, UK

SJG, 0000-0001-7042-7147

Past global warming events such as the Palaeocene–Eocene Thermal Maximum (PETM—56 Ma) are attributed to the release of vast amounts of carbon into the ocean, atmosphere and biosphere with recovery ascribed to a combination of silicate weathering and organic carbon burial. The phytoplanktonic nannoplankton are major contributors of organic and inorganic carbon but their role in this recovery process remains poorly understood and complicated by their contribution to marine calcification. Biocalcification is implicated not only in long-term carbon burial but also both short-term positive and negative climatic feedbacks associated with seawater buffering and responses to ocean acidification. Here, we use exceptional records of preserved fossil coccospheres to reconstruct cell size distribution, biomass production (particulate organic carbon, POC) and (particulate) inorganic carbon (PIC) yields of three contrasting

nannoplankton communities (Bass River—outer shelf, Maud Rise—uppermost bathyal, Shatsky Rise—open ocean) through the PETM onset and recovery. Each of the sites shows contrasting community responses across the PETM as a function of their taxic composition and total community biomass. Our results indicate that nannoplankton PIC:POC had no role in short-term climate feedback and, as such, their importance as a source of CO_2 to the environment is a red herring. It is nevertheless likely that shifts to greater numbers of smaller cells at the shelf site in particular led to greater carbon transfer efficiency, and that nannoplankton productivity and export across the shelves had a significant modulating effect on carbon sequestration during the PETM recovery.

This article is part of a discussion meeting issue 'Hyperthermals: rapid and extreme global warming in our geological past'.

1. Introduction

Past transient global-warming events such as the Palaeocene–Eocene Thermal Maximum (PETM) approximately 56 million years ago are attributed to the release of vast amounts of carbon into the ocean, atmosphere and biosphere with the recovery of the Earth system largely ascribed to increased weathering of silicates and/or increased rates of organic carbon burial [1,2]. However, the relative contributions of these feedback mechanisms and how and when they operated within the tens to hundreds of thousands of years that followed the onset of these events are still poorly constrained [1,3]. Evidence is primarily drawn from biogenic carbon, carbonate and barite accumulation rates, carbon isotopes, palaeoecological trends and Earth system models [1–4]. The biotic proxies rely heavily on the robust and ubiquitous fossil records of calcareous nannoplankton (predominantly coccolithophores), planktonic and benthic foraminifera, and dinocysts. Despite some incongruities, the analysis of assemblage compositions and abundances has led to broad agreement on the marine response to the PETM, with increased productivity in coastal and continental margin regions but decreased productivity in the open ocean [4–8]. Palaeoecological analysis of nannoplankton has unpinned documentation of the spatial heterogeneity of biotic response at the PETM [4,7–12] but there have also been attempts to quantify rates of production/export through the event [4], and to uncover evidence of disruption of calcification brought on by changing atmospheric and ocean chemistry [4,13–15]. These endeavours are challenging given the potential biases in the fossil record, which become particularly acute during the PETM, as carbonate dissolution caused widespread modification of the preserved record and introduced uncertainties regarding carbonate production versus preservation [4]. Furthermore, the specific role of calcareous nannoplankton in any productivity-feedback on climate remains elusive because speculation surrounds the duplicity of nannoplankton calcification, with its theoretical counteracting effect on the short-term buffering capacity of surface waters (e.g. [16–21]), and whether this might have acted to reduce the effectiveness of plankton involvement in atmospheric CO_2 drawdown during the event. One avenue that has remained largely unexplored, however, is the extraction of detailed information on the cellular characteristics of these ancient plankton and how cells and communities of cells varied in space and time through these intervals of tumultuous environmental change. In particular, we have yet to document cell-size distributions or ratios of organic to inorganic carbon across ancient nannoplankton species and communities. As such, we currently have little to no appreciation of the calcareous nannoplankton contribution to carbon sequestration during extreme transient events like the PETM that we know are characterized by large shifts in assemblage composition. Here, we take advantage of exceptionally preserved nannoplankton records with unusually abundant occurrences of entire exoskeletons (coccospheres) that allow us to make direct measurements of cellular traits, such as cell volume and calcite mass, and, for the first time, to quantify cell-size frequency distributions across communities through the PETM event. Further, we extrapolate from these unique data to reconstruct population biomass for three distinct oceanographic settings (shelf, off-shelf and open

ocean), assessing the impact of climate change on these cellular characteristics and the significance of the changes for carbon sequestration and the Earth system feedbacks which operated during the recovery.

2. Material and methods

(a) Material

Our analytical approach (see §2c) requires the integration of PETM coccosphere measurements with fossil calcareous nannoplankton ('nannofossil') assemblage data. Fossil coccospheres allow us to document cell size, coccosphere geometry and exoskeletal calcite mass, and assemblage data provide relative abundance distributions of nannoplankton communities across both space and time. Preservation of coccospheres is not typical in nannofossil records and requires targeting samples that satisfy a number of taphonomic requirements, usually including clay-rich host sediments, shallow burial-depths and low bioturbation-intensity [22]. Here our coccosphere data come from sites with exceptional nannofossil preservation, including Bass River and Wilson Lake (New Jersey), Lodo and Tumey Gulches (California), ODP Site 401 (Bay of Biscay), and Kilwa (Tanzania) [22] (examples in figure 1). High numbers of PETM-interval coccospheres were present at all these sites and some data were previously presented in [23,24]. Our (published) assemblage data come from three sites that lie in distinctly different settings of the PETM marine realm: Bass River, a mid-latitude, high-productivity shelf setting off the North American seaboard (onshore drillsite, ODP Leg 174AX [4]); Maud Rise, an off-shelf, high-latitude site in the south Atlantic sector of the Southern Ocean (ODP Site 690 [4]); and Shatsky Rise, an open-ocean, central gyre, low-latitude site in the Pacific (ODP Site 1209 [4,7]). For comparative purposes, the assemblage data are grouped into three key time-slices relative to the stratigraphy of the carbon isotope excursion (CIE) that defines the PETM [25–27]—the pre-CIE (the averaged assemblage composition from immediately below the first expression of the carbon isotope excursion), the peak of the PETM event (averaged assemblage composition across samples from within the core of the CIE before isotopic levels began to increase into the recovery interval), and the PETM recovery interval (averaged assemblage composition across samples within the core of the recovery phase where carbon isotope values were returning to, but had not yet reached, a stable post-event level).

(b) Fossil coccospheres, cell geometries and estimates of cellular PIC and POC levels

Fossil coccospheres were imaged from simple smear slides [28] using light microscopy at ×1000 magnification following the imaging and measurement procedures of [23] and [29]. Two images were taken of each coccosphere, one focused on the maximum outer coccosphere circumference, allowing for the coccosphere and cell dimensions to be measured (the internal dimension representing the position of the original cell), and the second focused on the proximal surface of the coccolith tube-cycle of a representative coccolith on the coccosphere surface, allowing for the coccolith dimensions to be measured. We collected additional disarticulated coccolith size data for each taxon from the same samples in order to determine the complete range of coccolith sizes present in each assemblage. As cell size and coccosphere size typically vary proportionally with coccolith dimensions [23,29,30], this enabled us to incorporate cell sizes that may not have been fully represented in the preserved coccosphere record (see §2c). We have supplemented these light microscope data with measurements and general observations from scanning electron microscope (SEM) imaging of rock-chip surfaces that allow *in situ* observations of nannofossils and coccospheres (see [31]).

The fossil record of coccospheres is dominated by coccolithophore taxa that form placolith-type coccoliths, which physically overlap and interlock to form a mechanically robust covering around the cell [22,23,30]. These placolith taxa are also often numerically dominant in nannoplankton assemblages and so for the majority of the PETM taxa we have direct coccosphere
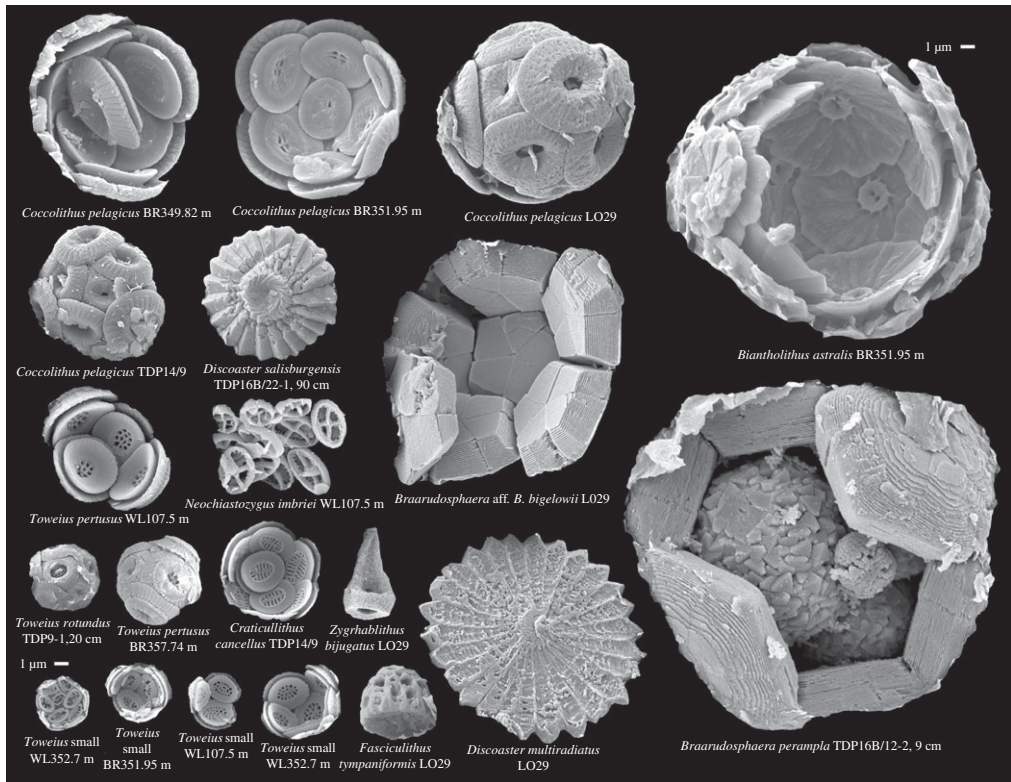
Figure 1. A representative selection of PETM coccosphere types and sizes, all shown on the same scale (scale bars are 1 μm). Also included are examples of a collapsed murolith coccosphere of *Neochiastozygus imbriei*, a disarticulated holococcolith of *Zygrhablithus bijugatus* and nannoliths of *Discoaster salisburgensis* and *D. multiradiatus* and *Fasciculithus tympaniformis*. Sample prefixes: WL—Wilson Lake, BR—Bass River, LO—Lodo Gulch, TDP—Tanzania Drilling Project.

measurements. The remaining nannoplankton groups present at this time form murolith coccoliths (disc-like morphologies), holococcoliths (often broadly disc-like) and nannoliths (non-coccolith morphologies), which lie side-by-side to form coccospheres structurally-bound by organic materials [22]. These taxa rarely or never survive as coccospheres in the fossil record and so we rely on modern analogue species, the observation of collapsed coccospheres, and/or geometric considerations in order to reconstruct coccosphere and cellular attributes (see electronic supplementary material). One exception to this is the Braarudosphaeraceae group whose coccospheres relatively frequently occur as fossils and for which we have direct measurements. The only common PETM holococcolith is the unusually large and robust species *Zygrhablithus bijugatus* and we have observed several collapsed coccospheres that have guided our coccosphere reconstructions. The PETM nannolith groups are dominated by *Discoaster*, *Fasciculithus* and *Sphenolithus*, all of which are extinct and have no appropriate extant analogue species. We have made the necessary assumptions that there are fundamental constraints on cell geometry imposed by nannolith morphology (especially lith curvature) and that most cells would have been spherical or sub-spherical as this is the most common cell shape across extant (and fossil) coccolithophores. Together, these direct coccosphere measurements and reconstructions allow us to document cell size (Θ), the taxon-specific relationship (the 'geometry') between number of coccoliths per cell (C_N), coccolith length (C_L) and Θ (table 1), and to calculate particulate organic carbon (POC) per cell and particulate inorganic carbon (PIC) per cell from these parameters (see electronic supplementary material).

Table 1. Summary of main biometric parameters measured or reconstructed from PETM coccospheres and loose coccoliths/nannoliths. C_N is the number of coccoliths per cell, Θ is cell diameter, and C_L is coccolith length.

taxon	lith type	mean C_N	C_N range	Θ range (μm)	C_L range (μm)[a]	geometry (power law relationship)[b]	shape factor[c]	
Coccolithus	placolith	12.9	6–23	3.3–18.2	2.1–12.9	$\alpha = 1.722, \beta = 0.417$	0.06	using modern *Coccolithus*
Toweius	placolith	7.2	5–14	2.7–12.1	1.6–8.3	$\alpha = 1.664, \beta = 0.418$	0.055	assuming slightly less calcified than *Coccolithus*
small *Toweius*	placolith	11.5	6–22	2.0–5.6	1.5–4.7	$\alpha = 1.664, \beta = 0.418$	0.055	assuming slightly less calcified than *Coccolithus*
Cruciplacolithus and *Campylosphaera*	placolith	14	8–25	4.3–12.9	3.8–8.7	$\alpha = 1.347, \beta = 0.408$	0.03	assuming significantly less calcified than *Coccolithus*
Cyclicargolithus	placolith	11.7	10–13	5.8–8.0	4.3–5.6	$\alpha = 1.909, \beta = 0.346$	0.08	using *Calcidiscus leptoporus*
Markalius	placolith	12	10–14	7.6–17.9	5.4–16.1	$\alpha = 0.580, \beta = 0.802$	0.07	assuming slightly more calcified than *Coccolithus*
Umbilicosphaera	placolith	6.6	6–9	2.9–4.8	2.9–5.0	too few coccospheres	0.015	using *Neosphaera coccolithomorpha*
Chiasmolithus	placolith	8.3	6–12	8.5–16.6	3.8–17.2	$\alpha = 1.608, \beta = 0.445$	0.06	using modern *Coccolithus*
Biscutum	placolith	19.5	14–25	12.1–20.8 (long axis)	4.9–7.2	$\alpha = 3.3815, \beta = 0.1916$	0.03	assuming significantly less calcified than *Coccolithus*; note that power law relationship less robust because cells are elongate and lith length less directly correlated with cell size.

(*Continued.*)

Table 1. (*Continued.*)

taxon	lith type	mean C_N	C_N range	Θ range (μm)	C_L range (μm)[a]	geometry (power law relationship)[b]	shape factor[c]	
Biantholithus	placolith	13	only 3 specimens	12.3–15.4	11.1–14.1	too few coccospheres	0.07	assuming slightly more calcified than *Coccolithus*
Braarudosphaera	nannolith	12	12	13.1–23.0	6.5–15.3	$\alpha = 1.780, \beta = 0.464$	n.a.	direct measurements from coccospheres/liths
Fasciculithus and *Sphenolithus*	nannolith	42.5	27–60*	14.0–29.4***	2.8–6.4 (base diameter)	$\Theta = 4.25C_L + 2.18$*	0.6–0.8	based on estimates herein of percentage space within a cone
Discoaster	nannolith	10.2	20–31*	5.1–26.1***	3.5–17.9 (rosette diameter)	$\Theta = 1.93C_L$*	0.04	using a 'rosette' morphology; shape factor based on half modern *Calcidiscus*
Muroliths	murolith	32.5	20–45**	9.7–25.6***	4.3–11.7	$\Theta = 2.13C_L + 0.48$*	0.035	based on volume calculation herein
Zygrhablithus bijugatus	holococcolith	32	32*	8.1–20.8***	2.9–7.4 (base diameter)	$\Theta = 2.8C_L$*	n.a.	using volume calculation herein of a simple base with a hollow, medium-sized spine

*Θ and C_N are from reconstructed coccospheres which for **murolith-bearing coccospheres which for ***murolith-bearing coccospheres are reconstructed based on modern analogues. [a]Lith size range is based on measurements of loose coccoliths in the same samples as where the coccospheres were found. [b]The calculation of cell size from coccosphere geometry takes the form $C_L = \alpha$ (cell surface area/C_N)$^\beta$. ****Geometries are simplified for murolith and nannolith-bearing taxa and assume a constant C_N. *****Geometries are after [32]. [c]Shape factors (k_S) are after [32] unless otherwise stated and are used to calculate cellular PIC via the equation ($k_S \times C_L^3$) × C_N × density calcite (ref. [32]).

rsta.royalsocietypublishing.org   *Phil. Trans. R. Soc. A* **376**: 20170075
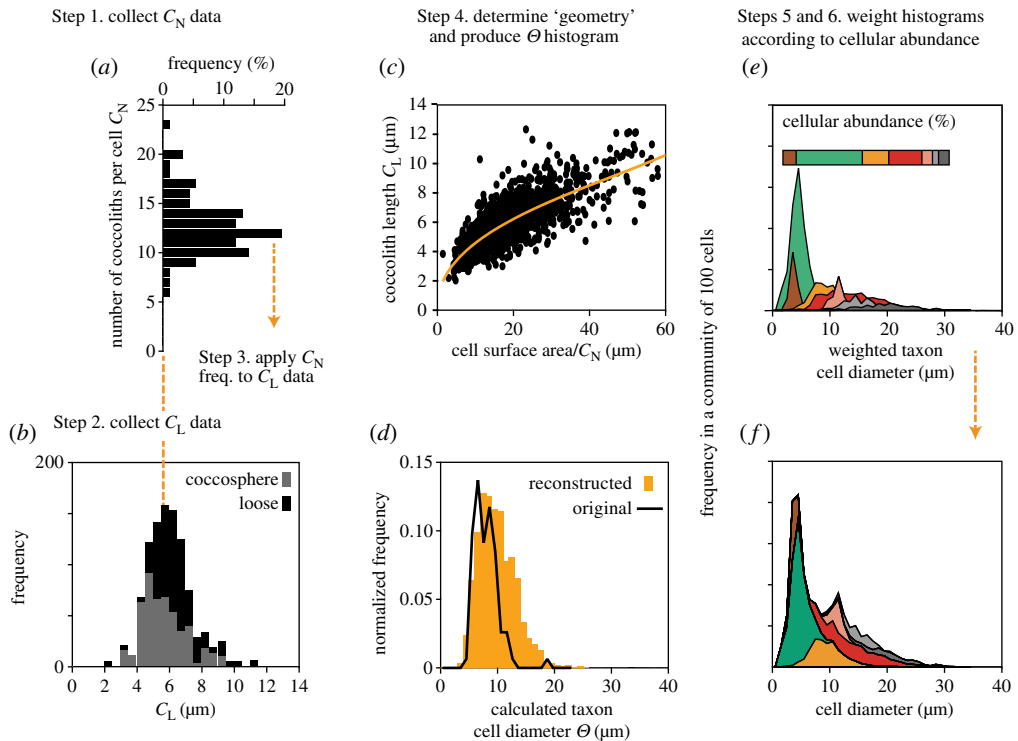
6

Figure 2. Illustrative schematic of the method used to reconstruct the frequency distribution of taxon cell size within each interval using fossil coccosphere geometry data. Firstly, the cell size distribution for each taxon is reconstructed based on measured fossil coccosphere geometry (*a*–*d*). The frequency distribution of number of coccoliths per cell (C_N) shown in (*a*) is applied to each size bin of the coccolith length (C_L) measured from loose coccoliths in the same assemblage (*b*, black histogram data) to calculate the number of cells of a particular taxon with specific combinations of C_N and C_L. The cell size of these combinations is calculated using a power-law relationship between cell size (Θ), C_L and C_N derived from fossil coccosphere measurements (*c*). The abundance of cells in each size class is then compiled to produce a frequency histogram of cell size for this taxon (*d*, orange histogram, as compared to the histogram of only measured fossil coccosphere cell sizes in black). Cell size histograms are then produced in the same way for all other taxa in the community. Site-specific community cell size is then reconstructed by weighting each taxon histogram by their relative cellular abundance in the community during each time interval (*e*) before stacking the frequencies in each size class (*f*) to produce an overall community cell size distribution.

(c) Reconstructing community cell size distribution and biomass

The distribution of cell sizes within a nannoplankton community is dependent on the frequency distribution of cell sizes within each species and the relative abundance of each of these species. Therefore, in order to reconstruct the cell-size frequency distribution of nannoplankton communities at our three sites (Bass River, Shatsky Rise, Maud Rise) we (i) derived the frequency distribution of cell sizes within each taxonomic group; (ii) normalized each cell-size histogram to the relative cell abundance of each taxonomic group; and then (iii) combined the abundance-normalized histograms of each taxonomic group to generate the cumulative cell-size frequency distribution for the total community.

For each taxon the method proceeds as follows (figure 2):

1. Plot the frequency distribution of C_N from fossil *coccosphere* geometry data (figure 2*a*).
2. Plot the frequency distribution of loose *coccolith* lengths (C_L) from the same samples (figure 2*b*). Measurements from an additional 100–300 loose coccoliths per taxon provide a necessary check on the expected range of cell sizes in each assemblage because preserved coccospheres tend to underrepresent the larger size classes.

3. Apply the C_N frequency plot across each C_L size bin, as extensive coccosphere geometry characterization of extant coccolithophores in culture show that the frequency distribution of C_N is consistent across the range of coccolith lengths [29]. As an illustrative example, imagine that 120 coccoliths in the assemblage fall within the 6.0–6.5 µm coccolith length category (e.g. figure 2*b*), and we know, from our C_N frequency plots of this taxon that 20% of the coccoliths (i.e. 24 coccoliths) in any C_L size bin are associated with cells that have 12 coccoliths per cell; this C_N–C_L combination would represent 2 cells formed of 12 coccoliths that are 6.0–6.5 µm in length. Of the remaining 96 coccoliths, the C_N histogram tells us that 18 coccoliths (15%) would be associated with cells that have 10 coccoliths per cell, thus representing 1.8 cells, and so on across the remaining C_N distribution. This is repeated for all of the C_L size bins until we know how many cells in the population of this taxon have x number of coccoliths of x µm in length.

4. Calculate the cell size of these C_L–C_N combinations using the taxon-specific power-law relationship (the 'geometry') that exists between C_N, C_L and Θ (figure 2*c*; table 1). This produces a histogram of cell size for each taxon (figure 2*d*). For the non-placolith taxa we applied a more basic geometry, derived using just one value of estimated C_N but again using measured loose coccoliths.

5. Introduce assemblage data by first converting *lith* per cent abundances into *cell* abundance using average lith number per cell per taxon (table 1).

6. Integrate resultant cell abundance and size distributions by weighting each cell-size histogram by its abundance in the community (figure 2*e*) and stacking the resultant histograms to produce the overall community cell size distribution (figure 2*f*).

7. Transform community cell size histograms into equivalent cell biomass where the area under the curve corresponds to the total biomass of 100 cells (expressed as organic carbon per cell) and the relative position along the axis corresponds to biomass distribution by equivalent cell size. The further to the right along the axis, the greater the proportion of biomass partitioned within larger cells.

(d) Calibrating nannofossil assemblages and nutrient availability

Our final step (step 8) scales the biomass plots according to estimated nannoplankton-biomass carrying capacity (effectively the nutrient availability) of the seawater at each site through time. We do this by adjusting the vertical amplitude of the biomass histograms in order to scale the total area under the curves with the relative level of surface-seawater biomass estimated for each site and for each time-slice. First, we place our sites on a common scale according to what the taxic composition of the assemblages tell us about nutrient regime. Specifically, we use the relative abundances of warm-water, oligotrophic-favouring-nannofossil taxa (*Discoaster*, *Fasciulithus*, *Sphenolithus* and *Coccolithus*) versus cooler-water, mesotrophic-favouring taxa (*Toweius* and *Chiasmolithus*) to form a palaeoenvironmental metric (the Palaeoenvironmental Index—PI) (modified from [4]; figure 3). Coccolithophores are strongly responsive to nutrient availability, favouring the same conditions as the majority of plankton, and they typically increase in abundance at the same time of year as increasing nutrients [33–35]. Therefore, we use the PI values as a means of quantifying relative differences in nutrient regime between our sites, with the differences in magnitude of the metric broadly consistent with our understanding of their latitude, nutrient availability and response to the PETM environmental change. This approach is also in general agreement with a previous attempt to scale export productivity changes across the PETM using biogenic barite [3]. We then calibrate our PI by placing estimated levels of nannoplankton standing cell-abundances per litre seawater (converted into biomass and expressed as organic carbon per millilitre of seawater) against our metric using modern shelf and gyre sites as equivalent end-member oceanographic settings. The values we use may not be wholly analogous for the Palaeogene oceans and biota, where, in particular, diatoms were less abundant, but they are a first order estimate of realistic variations. At the lower end of the scale for the pre-CIE PI value at the Shatsky Rise gyre site, we have placed a conservative estimate of 25 cells per millilitre
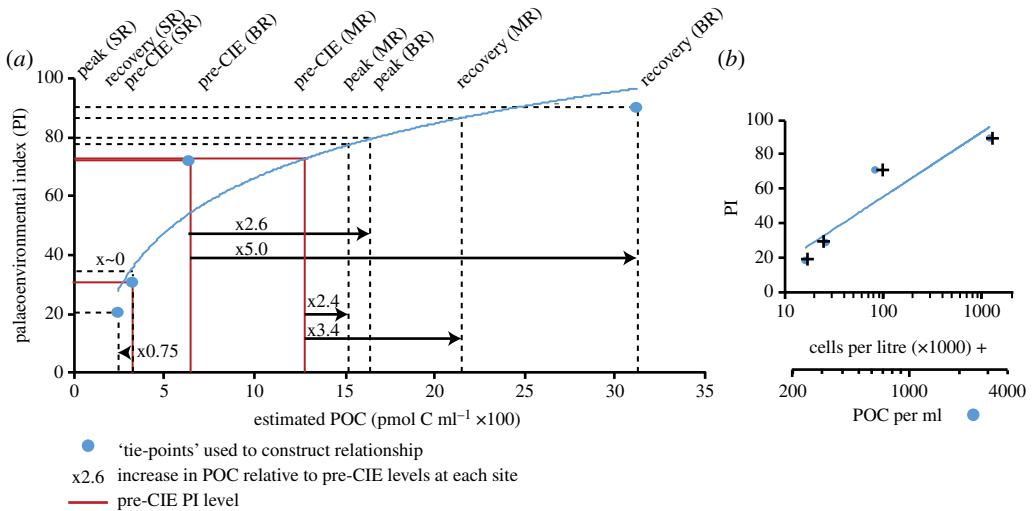
Figure 3. Calibrating the nannofossil-based palaeoenvironmental index (PI) with estimated levels of biomass in seawater, expressed as particulate organic carbon (POC, pmol C ml^{-1}). PI is calculated from nannofossil relative abundance data as total mesotrophic/eutrophic water-favouring nannofossil taxa divided by mesotrophic/eutrophic water-favouring taxa plus oligotrophic-favouring taxa with a value approaching 100 indicating dominance by mesotrophic/eutrophic favouring taxa. In (*a*), the red lines indicate the pre-CIE PI and resultant estimated POC values for each site and the times increases in POC for each site are relative to these pre-CIE values. The blue circles highlight the tie-points described in the text to construct the estimated PI to POC relationship. The dashed horizontal lines show the PI values for the non-tie-point time-slices from the three sites and the vertical dashed lines show the resultant estimated POC values. In (*b*) are the PI versus POC tie-points (both shown here on a log scale) with their equivalent cell numbers illustrating the close relationship between POC and cell numbers but demonstrating subtle differences that are because of variations in cell volume between the different tie-points.

based on measures of 25–35 cells ml^{-1} in modern subtropical gyres [36]; 25 cells ml^{-1}, using our Shatsky pre-CIE cell size community structure, corresponds to a total community biomass yield (our estimated nannoplankton carrying capacity) of 313 pmol POC ml^{-1}. We then impose an arbitrary reduction of a third of community biomass into the peak PETM, where nannofossil communities indicate reduced nutrient availability caused by warming and stratification [7]. Towards the upper end of the PI scale, we use a conservative 100 cells ml^{-1} for the pre-CIE PI value at Bass River, which corresponds to a community biomass of 630 pmol POC ml^{-1}. This is based on normal (non-bloom), coccolithophore cell-counts ranging from 70 to 100 cells ml^{-1} from the temperate, productive shelf-seas off the UK [35]. We then impose a conservative fivefold increase in community biomass reflecting the increased nutrient runoff across the event [7,26], based on the range of chlorophyll *a* measured on the UK shelf from the summer productivity minimum to the spring increase in nutrients, a range of 0.1 to 8.0 mg m^{-3} [37]. This is consistent with accumulation rate estimates of carbonate at Bass River, where rates increased from 0.16 to 1.86 g m^{-2} kyr^{-1} from pre-CIE to the peak of the CIE, approximately an order of magnitude increase, although some increase is due to enhanced carbonate preservation [26]. As PIC:POC in coccolithophores is generally close to 1 (figure 3) we can use carbonate accumulation to infer associated minimum levels of surface water POC. Using these values of community biomass/carrying capacity, the Shatsky Rise and Bass River end-members top and tail the PI calibration and allow us to scale the biomass histograms across the time-slices as well as placing biomass estimates on the intermediate PI values recorded at Maud Rise (figure 3).

3. PETM cellular communities and their biomass

The coccospheres we have imaged and measured from a range of sites provide us with accurate taxon-specific geometry characteristics, i.e. the fundamental coccosphere traits of how coccoliths

surround each cell and the cell-to-coccolith size relationship, as well as the frequency distributions of those relationships. The deviation of taxon averages from the overall trend line between cell size and coccolith size illustrates the taxon-specific ranges in geometries for our Palaeogene nannofossils, which are principally a function of varying numbers and degrees of overlap of coccoliths on the coccospheres (figure 4*a*,*b*). Those taxa that lie below the trend line have either high numbers of small coccoliths per cell (e.g. *Biscutum*) or relatively low levels of coccolith overlap on their coccospheres (e.g. *Umbilicosphaera*) (figure 4*b*). Correspondingly, the taxa that lie above the trend line have fewer, larger coccoliths for a given cell size (e.g. *Chiasmolithus*) or greater coccolith overlap (e.g. *Biantholithus*) (figure 4*b*). These subtle differences in the relationships between C_N, C_L and Θ give rise to the taxon-specific power relationships (table 1). Converted to cellular PIC and POC, these coccosphere data reveal that most cells lie at, or close to, a PIC:POC ratio of 1 (70% fall between 0.5 and 1.5), irrespective of cell size (figure 4*c*,*d*). Some taxa show averages that lie away from this line, for example, relatively lightly calcified forms with lower PIC:POC (e.g. *Campylosphaera* and *Biscutum)* lie below the 1:1 line, with ratios down to 0.06 (approximately 1:17), and more heavily calcified taxa (e.g. *Braarudosphaera* and *Biantholithus)* lie above the line with cells achieving, in some instances, unusually high PIC:POC ratios of up to 14. The similarity in position of taxon averages between figure 4*b* and 4*c* is in part because the POC axis and cell-size axis are recording essentially the same parameter, as our calculation of POC is based on cell volume [38]. But the position of the coccospheres on the C_L and PIC axes shows that taxa with fewer, larger coccoliths tend to have higher PIC:POC than those with greater numbers of smaller coccoliths. Because of this, the murolith taxa, with larger reconstructed cell sizes and higher numbers of smaller coccoliths, fall below the 1:1 line, averaging PIC:POC of between 0.8 and 0.36 (equivalent to a maximum of 1:3). Likewise, although the individual nannoliths of *Fasciculithus* and *Sphenolithus* are relatively heavily calcified, their high numbers on large cells result in estimated PIC:POC that is lower than might have been supposed, still close to the 1:1 line (PIC:POC estimates of 1.2–1.3).

The integration of cell sizes and calculated PIC and POC in our cellular community reconstructions illustrates that the size distributions across Palaeogene communities are strongly biased towards relatively small cell sizes, with modal cell diameters of 4–5 µm at all sites, although there is a broader cell-size range at open-ocean Shatsky Rise (figure 5*a*). Superficially, all three sites appear to show little variation in cell size distribution through time with no significant changes standing out. However, cell diameter hides the fact that larger cells, even if at low abundance, volumetrically outweigh smaller cells and this is clearly the case when we transform cell diameter data into cell biomass. This first set of biomass plots (figure 5*b*) illustrates the disproportionate contribution of the rarer but larger cells in the distribution of biomass across the cell-size range at a constant abundance. The impact of large cells is particularly prominent at Maud Rise, where the presence of *Chiasmolithus* results in the majority of community biomass packaged into a few, large cells. Likewise, at Bass River and Shatsky Rise, we see a significantly more balanced distribution of biomass across the community than is suggested by the cell diameters alone.

Across the time-slices at Shatsky Rise and Maud Rise, the community biomass structure of 100 cells remains relatively similar (total biomass shows little change), even though the taxa contributing biomass change significantly. For example, at Maud Rise, *Chiasmolithus* and *Zygrhablithus* show a large shift in abundance between the pre-CIE and peak-CIE time-slices but this has little effect on the overall biomass distribution across cell sizes. A greater difference through time is seen at Bass River, where biomass associated with larger cells declines in the PETM peak and recovery resulting in a greater than halving of total biomass per 100 cells. These plots with constant cell number are useful because they graphically illustrate how different the communities are between the sites in terms of how biomass is packaged across cells. However, they provide no information on variations in standing stock from site to site. Therefore, in figure 5*c* we have scaled the biomass plots according to estimated nutrient availability for each site and for each time-slice. The Bass River and Maud Rise communities show higher levels of inferred biomass per unit seawater than Shatsky Rise, up to at least 10 times higher in the
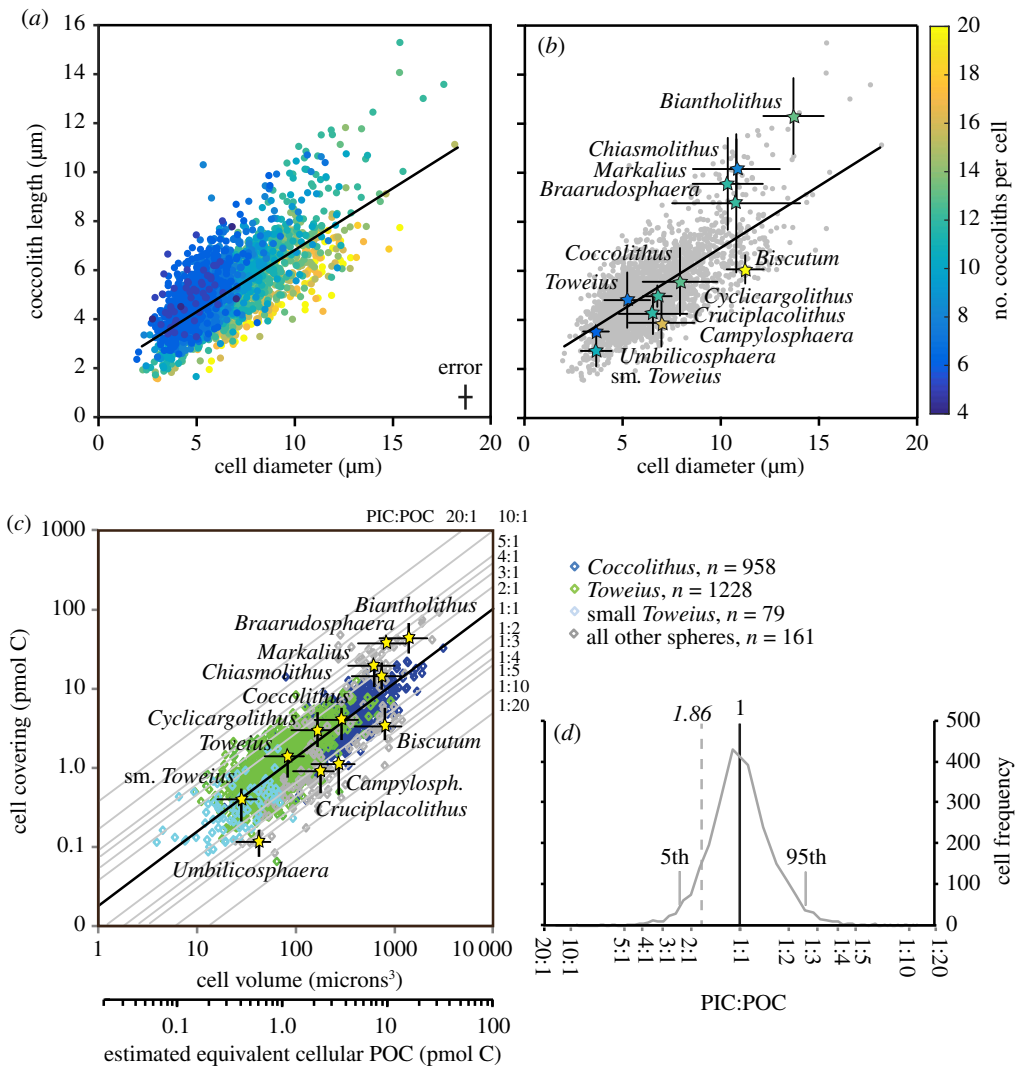
Figure 4. Coccosphere biometric data and calculated PIC and POC per cell for 2,426 PETM coccospheres. In (*a*) are plotted cell diameter (Θ) against coccolith length (C_L) for each coccosphere, and the number of coccoliths per coccosphere (C_N) indicated by the colour. The cell diameter of *Biscutum* are the diameters of spherical equivalents (because *Biscutum* cells are ovoid to cigar-shaped). In (*b*), the same data are shown with the means of each taxon highlighted (stars) and the 5–95% spread of the taxon size data indicated by the black bars. The colour of the star indicates average C_N. A broad correlation between coccosphere Θ and C_L is a persistent feature of coccosphere geometry (linear trend-line in *a* and *b*), with larger coccospheres typically associated with larger coccoliths. The notable scatter in the relationship between Θ and C_L is a result of varying C_N. In (*c*), all coccospheres have been converted into cell volume and estimated POC per cell and C_L and C_N have been combined to calculate PIC per cell. Diagonal lines indicate PIC to POC ratios. In (*d*) the PIC:POC of the coccospheres are shown as a frequency plot with the 5th and 95th percentiles indicated and the theoretical ratio of 1.86 where photosynthesis balances calcification resulting in no net carbon fixation [21]. The error/uncertainty black bars in (*c*) are the cumulative highest and lowest PIC and POC values we can calculate using all the uncertainties/errors listed below. Errors/uncertainties include direct measurements of Θ from the coccospheres (minimal measurement error with high reproducibility). Uncertainty with the counting C_N is minimal for low coccolith number—up to 9—increasing as the C_N increases, up to an uncertainly of approximately ±2 at a C_N around 18 upwards [23], resulting in under or overestimate in PIC of approximately $\pm7\%$ to approximately $\pm10\%$. Uncertainty associated with converting inner coccolith cycle (the parameter we can measure accurately on the coccospheres) to total C_L (which is obscured by coccolith overlap) is approximately 15%. Uncertainty associated with application of shape factors suggested by ref. [32] to be approximately 20%. Uncertainties in estimating POC from errors in Θ measurement are as above and uncertainty in the ref. [38] equation uses the published 95% confidence intervals.
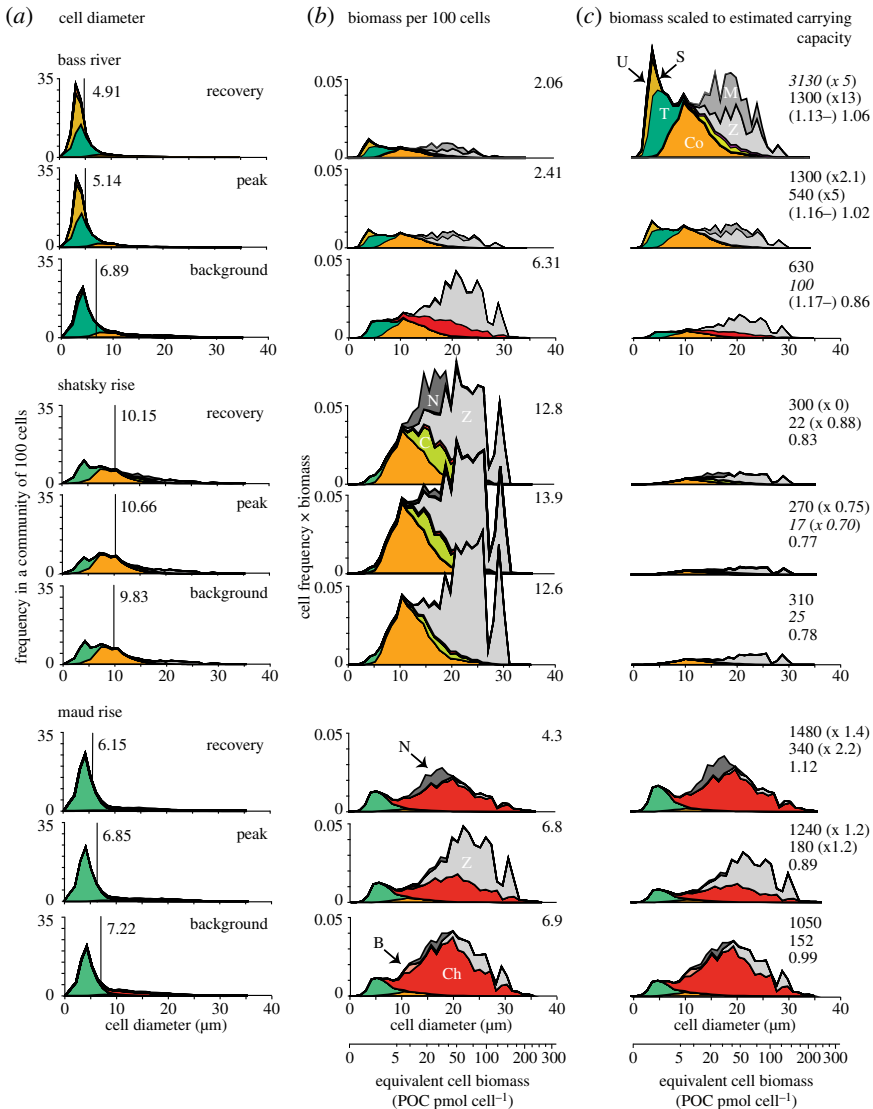
Figure 5. Reconstructed cellular communities and their biomass across three time-slices of the PETM—the pre-CIE (labelled background), the onset to peak of the CIE (labelled peak), and the recovery—from Bass River, Shatsky Rise (ODP Site 1209) and Maud Rise (ODP Site 690). In (*a*) are size frequency histograms of cell diameter (of 100 cells) with mean cell diameter noted in the vertical black line and value, separated into taxon by colour and with a prefix: U—*Umbilicosphaera*, S—small *Toweius*, T—*Toweius*, Co—*Coccolithus*, C—*Campylosphaera* and *Cruciplacolithus*, Ch—*Chiasmolithus*, B—*Biscutum*. In grey are the cell diameters for taxon that do not preserve as coccospheres: N—nannoliths (including *Discoaster*, *Sphenolithus* and *Fasciculithus*), M—muroliths, and Z—*Zyghrablithus*. In (*b*), cell diameter has been converted into cell biomass with the total area under the curves equalling total cell biomass and the distance along the *x* axis indicating how that biomass is distributed according to cell size. The value given is the total biomass of 100 cells. In (*c*), biomass from (*b*) has been scaled according to estimated changes in nutrient availability at each site and across the event. Again, the area under the curve corresponds to total biomass. The values on the right give amount of (pmol) POC per millilitre (top), number of cells per millilitre (middle), and community PIC:POC (the total PIC of 100 cells divided by the total POC of 100 cells, bottom). For the PIC:POC, in brackets is the PIC:POC of a 'bloom' end-member community dominated by a low diversity mesotrophic-eutrophic subset of the community. In brackets for the other two values are the times change from pre-CIE values. The values that are italicized indicate which values were used as tie-points in figure 3. For Bass River, the time-slices include data averaged across 358.94–357.56, 357.38–356.83, and 352.59–349.03 mbs; for Site 1209 across 216.80–216.36, 216.35–216.22, and 216.17–215.47 mcd, and for Site 690 across 172.33–171.43, 170.61–170.21, and 169.40–167.14 mbsf.

recovery interval. Bass River shows a marked increase in total biomass through the time-slices, which was part of our initial assumptions underlying figure 3. However, because of the shift in community cell size structure, this increase in biomass is accompanied by a huge increase in cell numbers, with a conservative estimate of a 13-fold increase (up to 1300 cells ml^{-1}) from pre-CIE values. This influx of small eutrophs (*Toweius*) is consistent with other evidence for an increase in productivity at Bass River, including total inorganic carbon accumulation [26] and biogenic magnetite [39]. If the productivity was strongly seasonal, as it may have been at Bass River where runoff was dependent on seasonal variations in precipitation [41], then these levels of cell numbers could certainly have approached a reasonable definition of a 'bloom'. If blooms did occur (see further discussion below), the communities were likely dominated by a mesotroph-eutroph subset of the assemblage, particularly *Toweius*, a scenario that is analogous to modern seasonal, nutrient-driven blooms of eutrophs in the related family Noelaerhabdaceae (e.g. *Emiliania* and *Gephyrocapsa*), which can reach in excess of a million cells per litre during a bloom [41,42].

A very different picture emerges at Shatsky Rise, a Pacific gyre site, where baseline standing stocks of cells would have been initially low and declined further at the peak of the PETM. Although similar overall size distributions were maintained throughout the event, this resulted in proportionally fewer cells when community biomass declined. The overall cell size character of the Shatsky Rise communities was very different to Bass River, with higher relative abundances of oligotrophs, such as *Discoaster* (and other nannoliths), and mesotrophs dominated by the large species *Coccolithus pelagicus*. A greater proportion of the POC was therefore packaged into larger cells. The same is true of the off-shelf site at Maud Rise where an increase in the large mesotrophic *Chiasmolithus* results in higher average cell-size and biomass. The Maud Rise communities do show some degree of change in cell-size distribution through the event, with an increase in cell numbers and a shift towards small-celled mesotrophs during the recovery phase, but not to the same extent as is seen at Bass River. The overall biomass estimates scaled to POC are, however, likely an overestimate at Maud Rise, with the higher PI values skewed because of temperature effects on the index.

The overall PIC:POC of these communities varies little across the event and between sites (figure 5). Bass River shows an increase from 0.86 to 1.06, reflecting a decline in contribution from lower PIC:POC nannoliths and holococcoliths in the community. The PIC:POC of just the *Toweius* taxa (shown in brackets in figure 5) illustrates a possible end-member bloom scenario. The Shatsky Rise community PIC:POC values are lower throughout the event (0.77–0.83) because of the persistent contribution of nannoliths, muroliths and holococcoliths, and the placoliths *Campylosphaera* and *Cruciplacolithus*. Maud Rise shows the largest change in PIC, from 0.89 to 1.12, mainly because of the increase in *Chiasmolithus*.

4. Discussion

(a) Calcareous nannoplankton productivity, calcification and climate feedbacks

It is likely that increased sequestration of carbon was a critical sink for high CO_2 across the PETM, in addition to the silicate weathering feedback that alone cannot account for the rapidity of climate recovery [1,2]. What remains uncertain is the extent to which calcareous nannoplankton productivity, export and burial influenced this process. Calcareous nannoplankton contribute both to the organic carbon pump and the carbonate counter pump and therefore play a multifarious role in carbon sequestration (e.g. [16–21]). They provide a direct, long-term sink for carbon through the production and burial of organic and inorganic matter and indirectly influence carbon export through the provision of ballasting minerals [17,19]. However, variations in coccolithophore calcification have been implicated in shorter-term surface water CO_2 buffering, because calcification reduces the rate at which the surface ocean can absorb atmospheric CO_2—the 'CO_2-calcification' feedback [18,19].

Our new data provide additional dimensions to the assessment of nannoplankton response and function at the PETM, allowing us to assess potential shifts in PIC:POC, cell-size distribution and biomass production. In the sections below we consider the potential influence of these combined factors on the production and export of carbon to the deep sea and hence the sign and strength of the resulting climate feedbacks.

(b) The role of nannoplankton PIC:POC in surface ocean buffering—the 'CO$_2$-calcification' feedback

A CO$_2$-driven reduction in coccolithophore calcification and hence increase in buffering capacity of surface waters would constitute a negative feedback to rising atmospheric CO$_2$ and *vice versa*, although the reality/magnitude of these feedbacks are contentious with a range of responses reported from culture experiments and the fossil record [19]. Culture manipulation experiments focusing on a limited number of extant taxa have largely, but not exclusively, reported reduced calcification under elevated CO$_2$ treatments, leading to a negative CO$_2$-calcification feedback hypothesis [16,19,43]. However, the opposite has also been argued, with [21] suggesting that increased coccolith calcification during high CO$_2$ intervals at glacial terminations may have constituted a positive feedback to increasing CO$_{2(atm)}$ on millennial timescales. At the PETM, while there are significant migration and population shifts across the event [7,8,44], there is little evidence for direct effects on calcification from surface water acidification [2,24] and therefore little obvious CO$_2$-calcification feedback. There are reports of morphologically-modified liths in one or two taxa (e.g. *Discoaster*, [14]) and minor changes in coccolith thickness [24], but these would have had little effect on the amounts of calcite being produced by these taxa, and overall the total nannoplankton population appears to have been little affected [15,44,45].

Our documentation of the PIC:POC character of the PETM nannoplankton community is the most comprehensive to date of its kind, and outstrips even our knowledge of modern coccolithophores. We have PIC:POC estimates for approximately 20 taxa from coccosphere observations and for nine taxa from coccosphere reconstructions, representing the majority of PETM diversity. The overwhelming outcome of this compilation is that the PIC:POC of most species is similar, with most lying within a narrow range from 0.5 to 1.5. The dominant taxa all have very similar PIC:POC with the more extreme end-member taxa limited to rare and/or sporadic occurrences (figure 4*c,d*). Therefore, even though our reconstructions of nannoplankton biomass across the PETM include evidence of significantly large changes, these do not translate into significant community PIC:POC variation, either through the time interval or even between our high-productivity and oligotrophic end-member sites. Overall, there is little scope for significant shifts in community PIC:POC unless the communities transitioned towards unrealistic species compositions; such as ones dominated by, for example, murolith-bearing coccolithophores (giving rise to lower PIC:POC) or *Biantholithus* or *Braarudosphaera* (giving rise to much higher PIC:POC). In reality, most sites at this time, regardless of latitude or nutrient regime, are dominated by varying proportions of *Toweius* and *Coccolithus* [44], both of which have similar cellular PIC:POC (despite different cellular levels of PIC and POC), with some degree of contribution by other placoliths, murolith and nannolith-bearing species. Our observations also indicate that shifts in community PIC:POC do not remotely approach the ratio of 1.86 where the balance of photosynthesis and calcification, in the most extreme scenario, results in no net carbon fixation [21]. The only other attempt to reconstruct coccolithophore PIC:POC through time reported similarly small variations across two Quaternary glacial termination events [21]. It is therefore hard to envisage how such small changes in PIC:POC could significantly alter overall nannoplankton calcite production and any minor variations in the amounts being produced per cell would be far outweighed by changes in species growth rates [24,29] or overall productivity. Given the narrow confines of nannoplankton PIC:POC diversity, the most significant influence on the rain ratio and associated buffering capacity would come from varying the ratio of calcifying

to all non-calcifying plankton, rather than any change within the nannoplankton themselves. For comparison, modern-day-equivalent total surface-water PIC:POC values, i.e. coccolithophores plus everything else, range from 0.001 to 0.4 [41,46], illustrating how small the coccolithophore inorganic carbon contribution can be, even taking into account the differences in plankton make-up between Palaeogene oceans and today. Therefore, while tendencies towards either more heavily/lightly calcified genotypes or species [47,48] may well be a response to seawater chemistry drivers, the hypothesis that the PIC:POC of nannoplankton/coccolithophores itself represents a significant feedback in the buffering capacity of the surface ocean appears to be a red herring.

(c) Nannoplankton cell size, biomass and export—the productivity feedback

The burial of organic and inorganic carbon in shelf environments increased by an order of magnitude across the PETM [26,49] amplifying the carbonate burial response to silicate weathering, and delivering a necessary additional sink for excess atmospheric CO_2. This increased burial of carbon, at least in part, could have resulted from higher levels of total plankton production and export [3], including calcareous nannoplankton, fuelled by increased runoff and nutrient supply [40]. The nannoplankton abundance data at Bass River confirm a shift to assemblages indicative of higher productivity but our community cell size record highlights the fundamental shift in population character, with a dramatic shift to smaller cell sizes and many more cells, equivalent in estimated cell numbers to modern bloom conditions.

The controls on plankton export are complex but could this shift in biomass packaging (towards smaller cells) further enhance the productivity feedback over and above the increased numbers, for example, by changing the effects of grazing, remineralization, or ballasting? On the one hand, smaller cells could be more easily recycled in surface waters, as well as being less effective ballasting agents. However, more importantly, there are significantly more cells being produced, increasing the likelihood of collision and aggregate formation, and hence enhancing carbon export/transfer efficiency [50,51]. Similarly, if these elevated cell numbers are associated with seasonally intensified bloom concentrations then this increase in biomass would promote greater levels of grazing (and increase contact/encounter rates) and the formation of faecal pellets that result in higher levels of transfer efficiency and less recycling.

(d) Evidence for changing export and transfer efficiency

It is difficult to unequivocally demonstrate the occurrence of bloom events in geological successions because the fossil record is typically time-averaged and so incapable of capturing very short-term phenomena (days to weeks). The exception to this are atypical laminated deposits that continuously record depositional processes and which remain undisturbed by mixing and/or bioturbation due to quiescent and hypoxic conditions. These exceptional sediments preserve records of exported aggregates and faecal pellets that are rich in microfossils (especially nannoplankton and diatoms) and in some cases the extent of these concentrations are considered to represent the fallout from bloom events (e.g. [31,52–54]). Although none of our successions are laminated in nature, both the Bass River and Lodo sediments are sufficiently undisturbed to reveal concentrations of nannoplankton that must represent exported aggregates and faecal pellets. In the case of Bass River, in particular, the coccolith concentrations are low diversity or monospecific and always dominated by *Toweius* species (figure 6), precisely as would be expected if these were blooms. This type of preservation is rare and often discontinuous (largely dependent on levels of bioturbation/oxygenation) and so we have been unable to systematically collect observations that provide comparative information throughout the PETM and across the different sites. However, the bulk of our faecal pellet/aggregate observations do come from the recovery interval of the PETM confirming that at this time there were low diversity assemblages, dominated by the principal eutroph group, *Toweius*, and exported to the seafloor in relatively large packages, indicative of effective transfer efficiency.
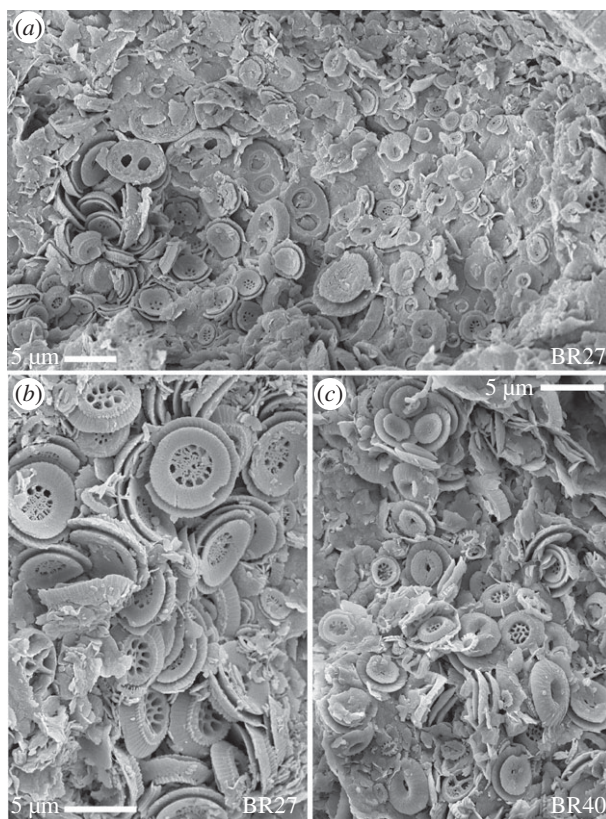
Figure 6. Scanning electron micrographs of fresh rock surfaces from the PETM recovery interval of Bass River with concentrations of coccoliths (mainly small and larger *Toweius*, including collapsed coccospheres), which represent aggregates or faecal pellets providing snapshots of the surface water populations. (*a*) and (*b*) are from two aggregations in sample BR27 (349.82 mbs) and (*c*) is an aggregation in sample BR40 (352.49 mbs).

Away from the shelf sites, there is evidence of a range of potential biological influence on carbon sequestration, dependent on oceanographic setting. Maud Rise appears to represent an intermediate productivity state between the shelf and open-ocean sites, and our cell size and biomass data would suggest a trend towards increasing biomass into the PETM event and a shift towards small-celled mesotrophs during the recovery phase. This shift towards the small mesotrophs is not as significant as that seen at Bass River, but nevertheless could be a biological amplifier to carbonate accumulation and is supported at Maud Rise by high nannofossil carbonate accumulation rates, perhaps again associated with increased runoff during the recovery phase [55].

At open-ocean Shatsky Rise, we see no evidence of increases in nannoplankton production and no major changes in cell size distribution during the recovery interval. Rather, the assemblage data here reveal greater proportions of oligotrophs [7] reflecting increased stratification and expansion of oligotrophic areas across the PETM [3,8,56]. In these settings it appears unlikely that nannoplankton primary production had any direct feedback-role on increased seafloor carbonate accumulation and that this was instead the result of enhanced calcite preservation as the calcite compensation depth (CCD) shoaled and ocean carbonate saturation increased, as is widely observed and modelled (e.g. [57,58]). Increased carbonate production could have accentuated CCD shoaling or contributed to higher accumulation rates above the CCD, but we think neither are likely given the minor changes in nannoplankton production and community cell-size structure, mirrored in the overall low estimates of export productivity in open ocean areas in general [3].

5. Summary and conclusion

Our fossil coccosphere geometry data provide new insights into the cellular-level response of this dominant plankton group during the PETM global warming event. We have been able to reconstruct the evolving cell-size distribution, biomass partitioning, and biomass and inorganic carbon yield of three contrasting fossil calcareous nannoplankton communities (shelf, off-shelf and open ocean) through the PETM onset and recovery, revealing distinctly different responses at each, consistent with previous palaeoecological data, and providing support for a significant plankton productivity feedback at this time. We document differences in numbers of cells and levels of cellular PIC and POC produced at our different sites, with the most dramatic changes across the PETM at the palaeo-shelf Bass River location. During the recovery interval, the Bass River nannoplankton community underwent a major shift towards increased production of smaller cells. However, despite these large changes in taxic composition and community structure, we see little significant difference in fundamental cellular PIC:POC, reflecting the underlying observation that the PIC:POC of most nannoplankton species is very similar. Given these results we consider the idea that nannoplankton PIC:POC might be a major control on surface water buffering and CO_2 drawdown, to be a red herring. Nevertheless, the cellular abundance and cell size changes likely modified food chain structure and export efficiency, providing a link between calcareous nannoplankton productivity, carbon sequestration and climate recovery. While the ultimate burial of carbon is what is fundamental to CO_2 removal and climate regulation, we need to further examine the potential implications of how calcareous nannoplankton/coccolithophore PIC and POC is packaged (how much and in what size cells) for ballasting and grazing and hence carbon export and export efficiency.

References

1. Bowen GJ, Zachos JC. 2010 Rapid carbon sequestration at the termination of the Palaeocene-Eocene Thermal Maximum. *Nat. Geosci.* **3**, 866–869. (doi:10.1038/ngeo1014)
2. Gutjahr M, Ridgwell A, Sexton PF, Anagnostou E, Pearson PN, Pälike H, Norris RD, Thomas E, Foster GL. 2017 Very large release of mostly volcanic carbon during the Palaeocene–Eocene Thermal Maximum. *Nature* **548**, 573–577. (doi:10.1038/nature23646)
3. Ma Z, Gray E, Thomas E, Murphy B, Zachos J, Paytan A. 2014 Carbon sequestration during the Palaeocene–Eocene Thermal Maximum by an efficient biological pump. *Nat. Geosci.* **7**, 382–388. (doi:10.1038/NGEO2139)
4. Gibbs SJ, Stoll HM, Bown PR, Bralower TJ. 2010 Ocean acidification and surface water carbonate production across the Paleocene-Eocene thermal maximum. *Earth Planet. Sci. Lett.* **295**, 583–592. (doi:10.1016/j.epsl.2010.04.044)
5. Thomas E. 2007 Cenozoic mass extinctions in the deep sea: What perturbs the largest habitat on Earth? In *Large ecosystem perturbations: causes and consequences*. Geological Society

of America Special Paper 424 (eds S Monechi, R Coccioni, MR Rampino), pp. 1–23. (doi:10.1130/2007.2424(01))

6. Sluijs A, Brinkhuis H. 2009 A dynamic climate and ecosystem state during the Paleocene-Eocene Thermal Maximum: inferences from dinoflagellate cyst assemblages on the New Jersey Shelf. *Biogeosciences* **6**, 1755–1781. (doi:10.5194/bg-6-1755-2009)

7. Gibbs SJ, Bralower TJ, Bown PR, Zachos JC, Bybell LM. 2006 Shelf and open-ocean calcareous phytoplankton assemblages across the Paleocene-Eocene Thermal Maximum: implications for global productivity gradients. *Geology* **34**, 233–236. (doi:10.1130/G22381.1)

8. Schneider LJ, Bralower TJ, Kump LR, Patzkowsky ME. 2013 Calcareous nannoplankton ecology and community change across the Paleocene-Eocene Thermal Maximum. *Paleobiology* **39**, 628–647. (doi:10.1666/12050)

9. Bralower TJ. 2002 Evidence of surface water oligotrophy during the Paleocene-Eocene Thermal Maximum: nannofossil assemblage data from Ocean Drilling Program Site 690, Maud Rise, Weddell Sea. *Paleoceanography* **17**, 1023. (doi:10.1029/2001PA000662)

10. Jiang S, Wise SW. 2007 Abrupt turnover in calcareous-nannoplankton assemblages across the Paleocene/Eocene Thermal Maximum: implications for surface water oligotrophy over the Kerguelen Plateau, Southern Indian Ocean. In *Antarctica: a keystone in a changing world—Online Proc. of the 10th ISAES* (eds AK Cooper, CR Raymond), USGS Open-File Report 2007-1047, Short Research Paper 024. Boulder, CO: GSA. (doi:10.3133/of2007-1047.srp024)

11. Angori E, Bernaola G, Monechi S. 2007 Calcareous nannofossil assemblages and their response to the Paleocene-Eocene Thermal Maximum event at different latitudes: ODP Site 690 and Tethyan sections. In *Large ecosystem perturbations: causes and consequences*. Geological Society of America Special Paper 424 (eds S Monechi, R Coccioni, MR Rampino), pp. 69–85. Boulder, CO: GSA. (doi:10.1130/2007.2424(04))

12. Agnini C, Fornaciari E, Rio D, Tateo F, Backman J, Giusberti L. 2007 Responses of calcareous nannofossil assemblages, mineralogy and geochemistry to the environmental perturbations across the Paleocene/Eocene boundary in the Venetian Pre-Alps. *Mar. Micropaleontol.* **63**, 19–38. (doi:10.1016/j.marmicro.2006.10.002)

13. Aze T *et al.* 2014 Extreme warming of tropical waters during the Paleocene-Eocene Thermal Maximum. *Geology* **42**, 739–742. (doi:10.1130/G35637.1)

14. Bralower TJ, Self-Trail JM. 2016 Nannoplankton malformation during the Paleocene-Eocene Thermal Maximum and its paleoecological and paleoceanographic significance. *Paleoceanography* **31**, 1423–1439. (doi:10.1002/2016PA002980)

15. Gibbs SJ, Bown PR, Ridgwell A, Young JR, Poulton AJ, O'Dea SA. 2016 Ocean warming, not acidification, controlled coccolithophore response during past greenhouse climate change. *Geology* **44**, 59–62. (doi:10.1130/G37273.1)

16. Zondervan I, Zeebe RE, Rost B, Riebesell U. 2001 Decreasing marine biogenic calcification— a negative feedback on rising atmospheric pCO_2. *Global Biogeochem. Cycles* **15**, 507–516. (doi:10.1029/2000GB001321)

17. Barker S, Higgins J, Elderfield H. 2003 The future of the carbon cycle: review, calcification response, ballast and feedback on atmospheric CO_2. *Phil. Trans. R. Soc. Lond. A* **361**, 1977–1999. (doi:10.1098/rsta.2003.1238)

18. Rost B, Riebesell U. 2004 Coccolithophores and the biological pump: responses to environmental changes. In *Coccolithophores: from molecular processes to global impact* (eds HR Thierstein, JR Young), pp. 99–125. Berlin, Germany: Springer.

19. Ridgwell A, Zondervan I, Hargreaves JC, Bijma J, Lenton TM. 2007 Assessing the potential long-term increase of oceanic fossil fuel CO_2 uptake due to CO_2-calcification feedback. *Biogeosciences* **4**, 481–492. (doi:10.5194/bg-4-481-2007)

20. Rickaby REM, Bard E, Sonzogni C, Rostek F, Beaufort L, Barker S, Rees G, Schrag DP. 2007 Coccolith chemistry reveals secular variations in the global ocean carbon cycle? *Earth Planet. Sci. Lett.* **253**, 83–95. (doi:10.1016/j.epsl.2006.10.016)

21. McClelland HLO, Barbarin N, Beaufort L, Hermoso M, Ferretti P, Greaves M, Rickaby REM. 2016 Calcification response of a key phytoplankton family to millennial-scale environmental change. *Sci. Rep.* **6**, 34263. (doi:10.1038/srep34263)

22. Bown PR, Gibbs SJ, Sheward R, O'Dea SA, Higgins D. 2014 Searching for cells: the potential of fossil coccospheres in coccolithophore research. *J. Nannoplankt. Res.* **34**, 5–21.

23. Gibbs SJ *et al.* 2013 Species-specific growth response of coccolithophores to Palaeocene–Eocene environmental change. *Nat. Geosci.* **6**, 218–222. (doi:10.1038/ngeo1719)

24. O'Dea SA, Gibbs SJ, Bown PR, Young JR, Poulton AJ, Newsam C, Wilson PA. 2014 Coccolithophore calcification response to past ocean acidification and climate change. *Nat. Commun.* **5**, 5363. (doi:10.1038/ncomms6363)

25. Bains S, Norris RD, Corfield RM, Faul KL. 2000 Termination of global warmth at the Palaeocene/Eocene boundary through productivity feedback. *Nature* **407**, 171–174. (doi:10.1038/35025035)

26. John CM, Bohaty SM, Zachos JC, Sluijs A, Gibbs S, Brinkhuis H, Bralower TJ. 2008 North American continental margin records of the Paleocene-Eocene thermal maximum: implications for global carbon and hydrological cycling. *Paleoceanography* **23**, PA2217. (doi:10.1029/2007PA001465)

27. Zachos JC, Wara MW, Bohaty S, Delaney ML, Petrizzo MR, Brill A, Bralower TJ, Premoli-Silva I. 2003 A transient rise in tropical sea surface temperature during the Paleocene-Eocene thermal maximum. *Science* **302**, 1551–1554. (doi:10.1126/science.1090110)

28. Bown PR, Young JR. 1998 Techniques. In *Calcareous nannofossil biostratigraphy* (ed PR Bown), pp. 16–28. London, UK: Chapman & Hall.

29. Sheward RM, Poulton AJ, Gibbs SJ, Daniels CJ, Bown PR. 2017 Physiology regulates the relationship between coccosphere geometry and growth phase in coccolithophores. *Biogeosciences* **14**, 1493–1509. (doi:10.5194/bg-14-1493-2017)

30. Henderiks J. 2008 Coccolithophore size rules—reconstructing ancient cell geometry and cellular calcite quota from fossil coccoliths. *Mar. Micropaleontol.* **67**, 143–154. (doi:10.1016/j.marmicro.2008.01.005)

31. Lees JA, Bown PR, Young JR, Riding JB. 2004 Evidence for annual records of phytoplankton productivity in the Kimmeridge Clay Formation coccolith stone bands (Upper Jurassic, Dorset, UK). *Mar. Micropaleontol.* **52**, 29–49. (doi:10.1016/j.marmicro.2004.04.005)

32. Young JR, Ziveri P. 2000 Calculation of coccolith volume and it use in calibration of carbonate flux estimates. *Deep Sea Res. Part II Top. Stud. Oceanogr.* **47**, 1679–1700. (doi:10.1016/S0967-0645(00)00003-5)

33. Daniels CJ, Poulton AJ, Esposito M, Paulsen ML, Bellerby R, St John M, Martin AP. 2015 Phytoplankton dynamics in contrasting early stage North Atlantic spring blooms: composition, succession, and potential drivers. *Biogeosciences* **12**, 2395–2409. (doi:10.5194/bg-12-2395-2015)

34. Hopkins J, Henson SA, Painter SC, Tyrrell T, Poulton AJ. 2015 Phenological characteristics of global coccolithophore blooms. *Global Biogeochem. Cycles* **29**, 239–253. (doi:10.1002/2014GB004919)

35. Mayers KM *et al.* In press Growth and mortality dynamics of spring coccolithophore populations in a temperate Shelf Sea (Celtic Sea, April 2015). *Prog. Oceanogr.* (doi:10.1016/j.pocean.2018.02.024)

36. Poulton AJ, Holligan PM, Charalampopoulou A, Adey TR. 2017 Coccolithophore ecology in the tropical and subtropical Atlantic Ocean: new perspectives from the Atlantic meridional transect (AMT) programme. *Prog. Oceanogr.* **158**, 150–170. (doi:10.1016/j.pocean.2017.01.003)

37. Poulton AJ, Davis CE, Daniels CJ, Mayers KMJ, Harris C, Tarran GA, Widdicombe CE, Woodward EMS. In press Seasonal phosphorus and carbon dynamics in a temperate shelf sea (Celtic Sea). *Prog. Oceanogr.* (doi:10.1016/j.pocean.2017.11.001)

38. Menden-Deuer S, Lessard EJ. 2000 Carbon to volume relationships for dinoflagellates, diatoms, and other protist plankton. *Limnol. Oceanogr.* **45**, 569–579. (doi:10.4319/lo.2000.45.3.0569)

39. Lippert PC, Zachos JC. 2007 A biogenic origin for anomalous fine-grained magnetic material at the Paleocene-Eocene boundary at Wilson Lake, New Jersey. *Paleoceanography* **22**, PA4104. (doi:10.1029/2007PA001471)

40. Zachos JC, Schouten S, Bohaty S, Quattlebaum T, Sluijs A, Brinkhuis H, Gibbs SJ, Bralower TJ. 2006 Extreme warming of mid-latitude coastal ocean during the Paleocene-Eocene Thermal Maximum: inferences from TEX86 and isotope data. *Geology* **34**, 737–740. (doi:10.1130/G22522.1)

41. Poulton AJ, Painter SC, Young JR, Bates NR, Bowler B, Drapeau D, Lyczsckowski E, Balch WM. 2013 The 2008 *Emiliania huxleyi* bloom along the Patagonian Shelf:

ecology, biogeochemistry, and cellular calcification. *Global Biogeochem. Cycles* **27**, 1023–1033. (doi:10.1002/2013GB004641)

42. Tyrrell T, Merico A. 2004 Emiliania huxleyi: bloom observation and the conditions that induce them. In *Coccolithophores: from molecular processes to global impact* (eds H Thierstein, JR Young), 585–604. Berlin, Germany: Springer.

43. Riebesell U, Zondervan I, Rost B, Tortell PD, Zeebe RE, Morel FMM. 2000 Reduced calcification of marine plankton in response to increased atmospheric CO_2. *Nature* **407**, 2–5.

44. Bown P, Pearson P. 2009 Calcareous plankton evolution and the Paleocene/Eocene thermal maximum event: new evidence from Tanzania. *Mar. Micropaleontol.* **71**, 60–70. (doi:10.1016/j.marmicro.2009.01.005)

45. Gibbs SJ, Bown PR, Sessa JA, Bralower TJ, Wilson PA. 2006 Nannoplankton extinction and origination across the Paleocene-Eocene Thermal Maximum. *Science* **314**, 1770–1773. (doi:10.1126/science.1133902)

46. Poulton AJ, Adey TR, Balch WM, Holligan PM. 2007 Relating coccolithophore calcification rates to phytoplankton community dynamics: regional differences and implications for carbon export. *Deep Sea Res. Part II Top. Stud. Oceanogr.* **54**, 538–557. (doi:10.1016/j.dsr2.2006.12.003)

47. Lohbeck KT, Riebesell U, Reusch TBH. 2012 Adaptive evolution of a key phytoplankton species to ocean acidification. *Nat. Geosci.* **5**, 346–351. (doi:10.1038/ngeo1441)

48. Beaufort L *et al.* 2011 Sensitivity of coccolithophores to carbonate chemistry and ocean acidification. *Nature* **476**, 80–83. (doi:10.1038/nature10295)

49. Speijer RP, Wagner T. 2002 Sea-level changes and black shales associated with the late Paleocene thermal maximum: Organic-geochemical and micropaleontologic evidence from the southern Tethyan margin (Egypt-Israel). In *Catastrophic events and mass extinctions: impacts and beyond*. Geological Society of America Special Paper 356 (eds C Koeberl, KG MacLeod), pp. 533–549. Boulder, CO: GSA.

50. Tréguer P *et al.* 2018 Influence of diatom diversity on the ocean biological carbon pump. *Nat. Geosci.* **11**, 27–37. (doi:10.1038/s41561-017-0028-x)

51. Bach LT, Boxhammer T, Larsen A, Hildebrandt N, Schulz KG, Riebesell U. 2016 Influence of plankton community structure on the sinking velocity of marine aggregates. *Global Biogeochem. Cycles* **30**, 1145–1165. (doi:10.1002/2016GB005372)

52. Kemp AES, Pike J, Pearce RB, Lange CB. 2000 The 'Fall dump'—a new perspective on the role of a 'shade flora' in the annual cycle of diatom production and export flux. *Deep Sea Res. Part II Top. Stud. Oceanogr.* **47**, 2129–2154. (doi:10.1016/S0967-0645(00)00019-9)

53. Davies A, Kemp AES, Pike J. 2009 Late Cretaceous seasonal ocean variability from the Arctic. *Nature* **460**, 254–258. (doi:10.1038/nature08141)

54. Thomsen E. 1989 Seasonal variation in boreal Early Cretaceous calcareous nannofossils. *Mar. Micropaleontol.* **15**, 123–152. (doi:10.1016/0377-8398(89)90008-X)

55. Zachos JC *et al.* 2005 Rapid acidification of the ocean during the Paleocene-Eocene Thermal Maximum. *Science* **308**, 1611–1615. (doi:10.1126/science.1109004)

56. Winguth AME, Thomas E, Winguth C. 2012 Global decline in ocean ventilation, oxygenation, and productivity during the Paleocene-Eocene Thermal Maximum: implications for the benthic extinction. *Geology* **40**, 263–266. (doi:10.1130/G32529.1)

57. Penman DE *et al.* 2016 An abyssal carbonate compensation depth overshoot in the aftermath of the Palaeocene–Eocene Thermal Maximum. *Nat. Geosci.* **9**, 575–581. (doi:10.1038/ngeo2757)

58. Kelly DC, Zachos JC, Bralower TJ, Schellenberg SA. 2005 Enhanced terrestrial weathering/runoff and surface ocean carbonate production during the recovery stages of the Paleocene-Eocene thermal maximum. *Paleoceanography* **20**, PA4023. (doi:10.1029/2005PA001163)